Exact and approximate fluxonium array modes

Stephen Sorokanich,[1,*] Max Hays,[2,†] and Neill C. Warrington[3,‡]

[1]Applied and Computational Mathematics Division, National Institute of Standards and Technology, Gaithersburg, Maryland 20899-8910, USA

[2]Research Laboratory of Electronics, Massachusetts Institute of Technology, Cambridge, Massachusetts 02139, USA

[3]Center for Theoretical Physics, Massachusetts Institute of Technology, Cambridge, Massachusetts 02139, USA

(Received 20 July 2024; accepted 17 August 2024; published 4 September 2024)

We present an exact solution for the linearized junction array modes of the superconducting qubit fluxonium in the absence of array disorder. This solution holds for arrays of any length and ground capacitance and for both differential and grounded devices. Array mode energies are determined by roots of convex combinations of Chebyshev polynomials, and their spatial profiles are modified plane waves. We also provide a simple, approximate solution which estimates array mode properties over a wide range of circuit parameters and an accompanying Mathematica file that implements both the exact and approximate solutions.

DOI: 10.1103/PhysRevB.110.125404

I. INTRODUCTION

The Josephson junction is arguably the most important building block of modern superconducting circuits. Large arrays of junctions have found applications in quantum information processing, quantum metrology, quantum-limited amplification, and many-body simulation [1–4]. In superconducting quantum computing, serially connected arrays of junctions are used to create so-called *superinductors*, reactive elements with impedances greater than the resistance quantum [5,6]. Along with single junctions and capacitors, superinductors compose the contemporary toolbox of circuit elements from which superconducting qubits are constructed. Superinductors are critical components of certain species of qubits such as the fluxonium, $\cos 2\phi$, and zero-π [7–9].

While it is often sufficient to treat a junction-array-based superconductor as a single linear inductor, it is important to remember that the phase drop across each junction in the array is fundamentally a separate degree of freedom. Noise coupled to these degrees of freedom can lead to decoherence of a qubit encoded in the circuit, for instance, via the Aharonov-Casher effect [10–13]. Moreover, these internal degrees of freedom of the superinductor are strongly coupled, forming higher-order array modes of the circuit. When designing qubit circuits, one typically wishes to keep the frequency of these array modes much higher than the system temperature, such that they can be safely neglected when considering the circuit dynamics. However, accurately predicting the array mode frequencies requires solving the full Hamiltonian of the circuit, including the degrees of freedom associated with the many junctions of the superinductor.

*Contact author: stephen.sorokanich@nist.gov
†Contact author: maxhays@mit.edu
‡Contact author: ncwarrin@mit.edu

In this paper, we focus on the array modes of fluxonium, a superconducting qubit formed by shunting a single junction with a superinductor and a capacitor [7] [see Fig. 1(a)]. When constructing the superinductor from serially connected junctions, it is typical to choose device parameters such that a single dominant mode, the *superinductance mode*, corresponding to a correlated fluctuation of phases across the entire array, governs the low-energy behavior, while all other modes, the so-called *array modes*, have higher energies and are thus comparatively suppressed. The low-energy Hamiltonian for the superinductance mode is simple compared with the full Hamiltonian and is given by

$$H = -4E_C\partial_\varphi^2 - E_J\cos(\varphi - \varphi_{\text{ext}}) + \frac{E_L}{2}\varphi^2, \tag{1}$$

where E_C, E_J, E_L are the effective capacitive, Josephson, and inductive energies; and φ_{ext} is related to the external flux threading the loop through $\varphi_{\text{ext}} = 2\pi\Phi_{\text{ext}}/\Phi_0$, where $\Phi_0 = h/2e$ is the superconducting flux quantum. While this Hamiltonian has been used to describe the dynamics of fluxonium devices with great success [7,14,15], for a more complete representation of the device physics, one must treat the phase drop across each array junction as a separate degree of freedom [6,12,16–18]. These considerations become especially important as E_L shrinks (inductance grows) because the array modes generally move to lower energy and thus become progressively more relevant to the circuit dynamics.

Here, we present an analytic solution to the array modes of the fluxonium model schematically depicted in Fig. 1(b). Previous theoretical works have used various approximations to examine the structure and noise properties of fluxonium array modes [6,12,16–18]. Building off these works, we present an analytic solution to array modes of the full fluxonium Hamiltonian as well as a useful approximation scheme. This exact solution also applies to the array modes of SNAILs [19]. In Sec. II, we define the model, tracking the effect of array modes on the quantum Hamiltonian. In Sec. III, we derive

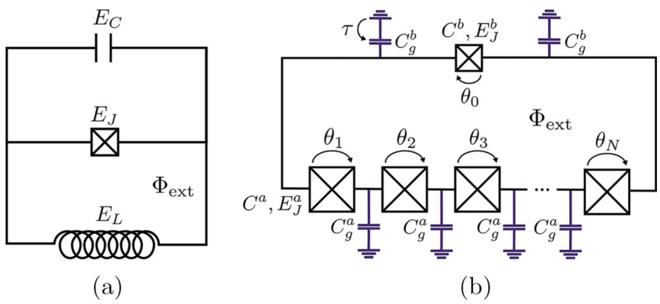

FIG. 1. (a) Simplified fluxonium circuit diagram. (b) Full fluxonium circuit diagram. Array junctions are assumed to have identical capacitances and Josephson energies, C^a, E_J^a, while the smaller junction has different values C^b, E_J^b (to simplify the diagram, we include any capacitance shunting the small junction in C^b). Similarly, the array junctions are supposed to couple to ground through capacitances C_g^a, while the smaller junction couples to ground capacitance C_g^b (shown in purple). An external flux $\Phi_{\rm ext}$ threads the loop.

the exact array modes of a differential fluxonium device in the presence of ground capacitances, then show how the array modes of a grounded fluxonium device is contained in this result. In Sec. IV, we present a simple approximation scheme for array modes. In Sec. V, we present our conclusions.

II. FLUXONIUM

A diagram of fluxonium is shown in Fig. 1: It consists of a single superconducting loop containing $N+1$ junctions threaded by an external flux $\Phi_{\rm ext}$. Indicated in the figure, θ_0 represents the gauge-invariant branch phase across the small junction, while $\theta_1, \dots, \theta_N$ represent phases across the N array junctions. The phases are constrained by the fluxoid quantization condition to satisfy $\sum_{m=0}^{N}\theta_m + \varphi_{\rm ext} = 2\pi z,\ z \in \mathbb{Z}$, and we employ this condition from the beginning to eliminate θ_0 from all expressions.

In this paper, we consider differential, or floating, fluxonium, where the overall voltage may fluctuate in time. This is reflected by the presence of the τ variable in Fig. 1, which is a reference node variable such that $\dot{\tau} \neq 0$. Grounded fluxonium devices, on the other hand, have $\dot{\tau} = 0$. Both grounded and differential devices are being built today [14,20], and interestingly, the array mode physics of a grounded fluxonium circuit is contained in that of the differential one in the absence of array disorder. While our analysis focuses on differential fluxonium, we show at the end of the next section how the grounded one can be obtained from the differential case.

We denote the Lagrangian of a differential fluxonium device by

$$L = T - U, \tag{2}$$

where T, U are the kinetic and potential energies, respectively. We consider a potential energy:

$$U = -E_J^a \sum_{m=1}^{N} \cos(\theta_m) - E_J^b \cos\left(\sum_{m=1}^{N}\theta_m - \varphi_{\rm ext}\right), \tag{3}$$

and kinetic energy $T = T_0 + T_g$, where

$$T_0 = \frac{1}{2}\left(\frac{\hbar}{2e}\right)^2 \left[C^a \sum_{i=1}^{N} \dot{\theta}_i^2 + C^b\left(\sum_{i=1}^{N}\dot{\theta}_i\right)^2\right]$$

$$T_g = \frac{1}{2}\left(\frac{\hbar}{2e}\right)^2 \left[C_g^a \sum_{i=1}^{N-1}\left(\dot{\tau} + \sum_{j=1}^{i}\dot{\theta}_j\right)^2 \right.$$

$$\left. + C_g^b \dot{\tau}^2 + C_g^b\left(\dot{\tau} + \sum_{j=1}^{N}\dot{\theta}_j\right)^2\right]. \tag{4}$$

This system has been previously considered [16,17]. Here, T_0 represents the kinetic energy of the junctions themselves, while T_g models capacitive coupling to ground [11,21–23]. The terms in T_g are represented by the purple capacitors in Fig. 1. The first term of T_g, proportional to C_g^a, accounts for ground capacitances along the array and is represented the purple capacitors at the bottom of the figure. The two remaining terms, proportional to C_g^b, account for ground couplings of the small junction and are represented by the purple capacitors at the top of the figure.

We emphasize that we are not considering the most general model of fluxonium: We assume zero array disorder. We make this assumption to obtain an analytic solution for array modes. A more realistic model incorporating array disorder was solved previously [12]. This solution is complementary to ours, providing a semianalytic solution to a more general case.

Our aim is to provide exact expressions for the array modes of the model of fluxonium model defined by Eqs. (2)–(4). These arise in the course of *circuit quantization*, a general method for formulating quantum theories of circuits [22,24]. The method proceeds in two steps: First, the classical Lagrangian is transformed into a classical Hamiltonian through a Legendre transformation, and second, the theory is quantized by promoting all dynamical variables appearing in the Hamiltonian to operators on a Hilbert space and by imposing on conjugate variables the canonical commutation relations.

The first step, Legendre transforming from Lagrangian to Hamiltonian, is complicated by the coupling between phase variables in Eq. (4). To accomplish this transformation, we proceed as follows [25]. We first rewrite the kinetic energy as

$$T = \frac{1}{2}\left(\frac{\hbar}{2e}\right)^2 \dot{x}^T \mathbb{M} \dot{x}, \tag{5}$$

where $x := (\tau, \theta_1, \dots, \theta_N)$. The $(N+1)\times(N+1)$ matrix $\mathbb{M}$ is equal to

$$\mathbb{M} = \begin{bmatrix} a & b^T \\ b & C \end{bmatrix}, \tag{6}$$

where $a = 2C_g^b + (N-1)C_g^a$ is a number, b is a vector with components $b_m = C_g^b + C_g^a(N-m)$, $(m = 1, \dots, N)$, and $C = C_1 + C_2 + C_3$ is an $N \times N$ matrix. Here, $(C_1)_{ij} =$

$C^a\delta_{ij}$, $(C_2)_{ij} = C^b + C_g^b$, and

$$C_3 = C_g^a \begin{bmatrix} N-1 & N-2 & \dots & 1 & 0 \\ N-2 & N-2 & \dots & 1 & 0 \\ \vdots & \vdots & \ddots & \vdots & \\ 1 & 1 & \dots & 1 & 0 \\ 0 & 0 & \dots & 0 & 0 \end{bmatrix}.$$

Since the potential energy Eq. (3) is independent of τ, its conjugate momentum is conserved, and τ can be eliminated from the Lagrangian entirely. Defining the total charge:

$$n_{\rm tot} = \frac{\partial L}{\partial \dot{\tau}} = 0, \tag{7}$$

one finds $\dot{\tau} = -a^{-1}b^T\dot{\theta}$, where $\theta := (\theta_1, \dots, \theta_N)$. Using this relation to eliminate $\dot{\tau}$ from the Lagrangian, one obtains

$$L = \frac{1}{2}\left(\frac{\hbar}{2e}\right)^2 \dot{\theta}^T \mathbb{C}\dot{\theta} - U, \tag{8}$$

where $\mathbb{C} = C + C_4$, $C_4 = -bb^T/a$. We have checked that $\mathbb{C}$ is the same capacitance matrix as in Ref. [16] (using their Eq. D3). Defining conjugate momenta $p_i = \partial L/\partial\dot{\theta}_i$ and performing the Legendre transformation, one finally obtains the classical Hamiltonian:

$$H = \frac{1}{2}\left(\frac{2e}{\hbar}\right)^2 p^T\mathbb{C}^{-1}p + U. \tag{9}$$

Having computed the classical Hamiltonian, one may quantize the theory. What results is a challenging quantum many-body problem which we do not attempt to solve (many-body calculations do exist, though, for example, the tensor network calculations of Ref. [12]). Instead, we focus on exactly computing the array modes and tracking their effect on the quantum theory. To accomplish the latter, we express all quantities in terms of the eigenvalues and normalized eigenvectors of $\mathbb{C}^{-1}$, which we denote as λ_m and v_m, and solve for in the following section.

We begin by defining a diagonal matrix $\Lambda_{mn} = \lambda_m\delta_{mn}$ and an orthogonal matrix $\mathbb{V}_{mn} = (v_m)_n$, so that $\mathbb{C}^{-1} = \mathbb{V}^T\Lambda\mathbb{V}$ and $\mathbb{V}^T\mathbb{V} = \mathbb{1}$. Defining new canonically conjugate variables $P = \mathbb{V}p$ and $\Theta = \mathbb{V}\theta$, one has $p^T\mathbb{C}^{-1}p = P^T\Lambda P$ and

$$\theta_m = \sum_{a=1}^{N}\Theta_a\mathbb{V}_{am},$$
$$\sum_{m=1}^{N}\theta_m = \Theta_0\sum_{b=1}^{N}\mathbb{V}_{0b} + \sum_{\mu=1}^{N-1}\sum_{b=1}^{N}\Theta_\mu\mathbb{V}_{\mu b}. \tag{10}$$

Promoting conjugate variables to operators satisfying $[\Theta_m, P_n] = i\hbar\delta_{mn}$ and defining

$$\varphi = \Theta_0\sum_{b=1}^{N}\mathbb{V}_{0b},$$
$$\mathcal{N}^{1/2} = \sum_{b=1}^{N}\mathbb{V}_{0b},$$
$$\mathcal{N}_\mu^{1/2} = \sum_{b=1}^{N}\mathbb{V}_{\mu b}, \tag{11}$$

one obtains the quantum Hamiltonian for fluxonium:

$$\begin{aligned}\hat{H} = &-4E_C\partial_\varphi^2 - 4\sum_{\mu=1}^{N-1}E_\mu\partial_\mu^2 \\ &-E_J^a\sum_{m=1}^{N}\cos\left(\varphi\frac{\mathbb{V}_{0m}}{\mathcal{N}^{1/2}} + \sum_{\mu=1}^{N-1}\Theta_\mu\mathbb{V}_{\mu m}\right) \\ &-E_J^b\cos\left(\varphi - \varphi_{\rm ext} + \sum_{\mu=1}^{N-1}\Theta_\mu\mathcal{N}_\mu^{1/2}\right),\end{aligned} \tag{12}$$

where $E_C = \mathcal{N}e^2\lambda_0/2$, $E_\mu = e^2\lambda_\mu/2$, and $\partial_\mu = \partial/\partial\Theta_\mu$. Similar expressions for the fluxonium Hamiltonain were found previously [12].

At this point, no approximations have been made. When ground capacitances are zero, however, the eigensystem of $\mathbb{C}^{-1}$ simplifies. One finds that $\lambda_0 = 1/(C^a + NC^b)$ and $\lambda_\mu = 1/C^a$ for every μ; the eigenvector for the superinductance mode is constant, with components $(v_0)_m = \mathbb{V}_{0m} = N^{-1/2}$, and within the degenerate subspace, a basis of array modes can be chosen so that $(v_\mu)_m = \mathbb{V}_{\mu m} = (2/N)^{1/2}\cos[\mu\pi/N(m-\frac{1}{2})]$ [16]. Thus, $\mathcal{N} = N$, and $\mathcal{N}_\mu = 0$. This choice of array mode basis eliminates them from the final line of Eq. (12), simplifying the problem. We will show in the following section that ground capacitances produce a nondegenerate array mode spectrum whose eigenvectors are eigenstates of parity. The odd parity modes satisfy $\mathcal{N}_\mu = 0$; however, the even parity modes have $\mathcal{N}_\mu \neq 0$. This produces couplings between the superinductance and parity even array modes. As reported in Ref. [12], these interactions produce important corrections to the circuit Hamiltonian which vary exponentially with mode impedances.

Since $E_J^a \gg E_C^a$, it is common to expand the array mode cosines in Eq. (12) to second order:

$$-E_J^a\sum_{m=1}^{N}\cos\theta_m = -E_J^aN + \frac{E_J^a}{2}\theta^T\theta + O(\theta_m^4). \tag{13}$$

Performing this expansion and rewriting the E_J^b cosine with trigonometric identities, one obtains

$$\begin{aligned}\hat{H} = &-4E_C\partial_\varphi^2 - E_J\cos(\varphi-\varphi_{\rm ext}) + \frac{E_L}{2}\varphi^2 \\ &+\sum_{\mu=1}^{N-1}\left(-4E_\mu\partial_\mu^2 + \frac{E_J^a}{2}\Theta_\mu^2\right) \\ &-E_J\cos(\varphi-\varphi_{\rm ext})\left[\cos\left(\sum_\mu\Theta_\mu\mathcal{N}_\mu^{1/2}\right) - 1\right] \\ &+E_J\sin(\varphi-\varphi_{\rm ext})\sin\left(\sum_\mu\Theta_\mu\mathcal{N}_\mu^{1/2}\right),\end{aligned} \tag{14}$$

where $E_J = E_J^b$, and $E_L = E_J^a/\mathcal{N}$. The first line is Eq. (1), with the relations between E_C, E_J, E_L and microscopic parameters now obtained. The remaining terms in the Hamiltonian describe array modes and intermode couplings [18].

Examining the Hamiltonian, one can see how the parameters of fluxonium are renormalized through various effects. For example, the inductive energy is given by $E_L = E_J^a/\mathcal{N}$, and only if the superinductance mode has a flat voltage profile does $\mathcal{N} = N$, producing the usual relationship $E_L = E_J^a/N$. In general, $\mathcal{N} \leqslant N$, raising the inductive energy. The quartic (and higher-order) couplings that we have dropped further renormalize E_L.

The renormalization of other couplings, such as E_J, can be compactly expressed in terms of the plasma frequencies and zero-point fluctuations:

$$\hbar\omega_\mu = \left(8E_\mu E_J^a\right)^{1/2} = \left(4E_J^a e^2\lambda_\mu\right)^{1/2},$$
$$\Theta_{\mu,\mathrm{zpf}} = \left(\frac{2E_\mu}{E_J^a}\right)^{1/4} = \left(\frac{e^2\lambda_\mu}{E_J^a}\right)^{1/4}. \tag{15}$$

Assuming array modes occupy their ground state,

$$\left\langle \cos\left(\sum_{\mu,b}\Theta_\mu \mathbb{V}_{\mu b}\right) - 1\right\rangle \simeq -\frac{1}{2}\sum_\mu \mathcal{N}_\mu \Theta_{\mu,\mathrm{zpf}}^2 .$$

Thus, to leading order in fluctuations, E_J is renormalized as

$$E_J \to E_J\left(1 - \frac{1}{2}\sum_\mu \mathcal{N}_\mu \Theta_{\mu,\mathrm{zpf}}^2\right). \tag{16}$$

The eigensystem of $\mathbb{C}^{-1}$ is thus seen to affect many properties of fluxonium: the charging energies of array modes, the renormalization of Hamiltonian couplings, as well as dispersive couplings not discussed here [17]. The eigensystem has been analytically solved in several limits. The case $C^b = 0$ was solved in Ref. [6], where it was shown that the eigenvectors of $\mathbb{C}^{-1}$ are plane waves, and analytic expressions for the eigenvalues were found. The case $C_g^a = C_g^b = 0$ was solved in Ref. [16], and later work included some effects of charge noise [11]. Nonzero C^b and C_g^a, C_g^b complicate the theory. Leading-order interactions between the superinductance and array modes were computed in Ref. [17]. Recent work has developed a semianalytical solution for array modes which holds in the presence of ground capacitances and disorder and performs tensor network calculations of the resulting quantum many-body system [12].

In this paper, we derive analytic formulas for the eigensystem when $C^a, C^b, C_g^a, C_g^b \neq 0$. In addition to containing as limiting cases the results of Refs. [6,16], our formulas are useful for understanding physics that emerges from heavily grounded or very long arrays, where the eigensystem of $\mathbb{C}^{-1}$ deviates from previous results substantially.

III. EIGENSYSTEM OF $\mathbb{C}^{-1}$

In this section, we derive exact expressions for the eigensystem of $\mathbb{C}^{-1}$. We do so in two steps: We find a simple representation of $\mathbb{C}^{-1}$, then diagonalize it. Recall that

$$\mathbb{C} = C_1 + C_2 + C_3 + C_4. \tag{17}$$

It is beneficial to consider a partial sum of $\mathbb{C}$, particularly the inverse $(C_2 + C_3 + C_4)^{-1}$. It is straightforward to verify that

$$\frac{1}{C_2 + C_3 + C_4} = \frac{-\Delta(\epsilon, \epsilon')}{C_g^a}, \tag{18}$$

where

$$-\Delta(\epsilon,\epsilon') := \begin{bmatrix} 1+\epsilon & -1 & & & -\epsilon' \\ -1 & 2 & -1 & & \\ & \ddots & \ddots & \ddots & \\ & & -1 & 2 & -1 \\ -\epsilon' & & & -1 & 1+\epsilon \end{bmatrix} \tag{19}$$

is an $N \times N$ matrix, and

$$\epsilon = \frac{C_g^a}{C_g^b}\frac{C^b + C_g^b}{2C^b + C_g^b}, \quad \text{and} \quad \epsilon' = \frac{C_g^a}{C_g^b}\frac{C^b}{2C^b + C_g^b}. \tag{20}$$

We observe that $(C_2 + C_3 + C_4)^{-1}$ represents a discrete Laplace operator. The (1,1), (N, N), $(1, N)$, and $(N, 1)$ entries of the matrix encode boundary conditions satisfied by the corresponding continuous function on the interval. These boundary conditions will, in general, fix a linear combination of the solution and its derivative at the left/right endpoints (i.e., Robin-Robin boundary conditions). For example, when $\epsilon = 1$ and $\epsilon' = 1$, the matrix represents a one-dimensional (1D) Laplace operator with periodic boundary conditions. It is conceivable that non-nearest-neighbor couplings will lead to inverse capacitance matrices of a similar form but with further off-diagonal bands. We speculate that the methods presented in this section, which rely primarily on the structure of banded matrices, may be used to also solve these problems.

The eigensystem of $\mathbb{C}^{-1}$ can be derived by noting that if, for some vector v and scalar λ,

$$\frac{1}{C_2 + C_3 + C_4} v = \lambda v, \tag{21}$$

then

$$\frac{1}{C_1 + C_2 + C_3 + C_4} v = \frac{\lambda}{1 + C^a\lambda} v, \tag{22}$$

which holds since C_1 is a multiple of the identity operator. Thus, is it enough to compute the spectrum of $(C_2 + C_3 + C_4)^{-1}$, and hence $-\Delta(\epsilon, \epsilon')$, to compute that of $\mathbb{C}^{-1}$. It is important to note that, while $1/(C_2 + C_3 + C_4)$ is sparse, $1/(C_1 + C_2 + C_3 + C_4)$ is dense, as can be seen by Taylor expanding in C_1 or numerically computing examples at small N. Thus, this seemingly trivial step is quite important for the analysis.

Before proceeding, we would like to point out that Eq. (18) itself is useful. The capacitance matrix itself is dense, and numerically computing its eigensystem becomes costly for long arrays: Eq. (18) shows the eigensystem can be computed from a sparse matrix.

We will now compute the eigensystem of $-\Delta(\epsilon, \epsilon')$. We will distinguish the eigenvalues of $-\Delta(\epsilon, \epsilon')$ and $\mathbb{C}^{-1}$, writing the former as ℓ and the latter as λ. For every eigenvalue ℓ of $-\Delta(\epsilon, \epsilon')$, the corresponding eigenvalue of $\mathbb{C}^{-1}$ is $\lambda = (C^a + C_g^a/\ell)^{-1}$. The eigenvectors of the two matrices are equal, and we denote these as v.

The eigensystem of $-\Delta(\epsilon,\epsilon')$ can be derived by exploiting reflection symmetry of the fluxonium circuit about its midpoint, which is present since we are considering a differential fluxonium circuit without array disorder. This symmetry is manifested in the fact that $-\Delta(\epsilon,\epsilon')$ commutes with

$$\mathbb{F} := \begin{bmatrix} & & 1 \\ & \iddots & \\ 1 & & \end{bmatrix}, \tag{23}$$

which implements the reflection. Since $\mathbb{F}^2 = \mathbb{1}$, the following matrices are projection operators:

$$P_\pm = \frac{1}{2}(\mathbb{1} \pm \mathbb{F}), \tag{24}$$

which allows $-\Delta(\epsilon,\epsilon')$ to be decomposed over subspaces as follows:

$$-\Delta(\epsilon,\epsilon') = \sum_{i=\pm} P_i\{-\Delta(\epsilon,\epsilon')\}P_i. \tag{25}$$

We call the P_+ subspace *parity even* and the P_- subspace *parity odd* (the voltage profiles of P_+ and P_- modes are, respectively, odd and even). Each term on the right-hand-side of Eq. (25) can be simplified:

$$P_\pm\{-\Delta(\epsilon,\epsilon')\}P_\pm = -\Delta(\epsilon_\pm,0)P_\pm, \tag{26}$$

where

$$\epsilon_+ := \epsilon - \epsilon' = \frac{C_g^a}{2C^b + C_g^b},$$
$$\epsilon_- := \epsilon + \epsilon' = \frac{C_g^a}{C_g^b}. \tag{27}$$

These expressions show that even modes depend on C^b, while odd ones do not, which is expected because only even modes drop in voltage across the small junction.

Denoting the eigenvectors of $-\Delta(\epsilon,\epsilon')$ which are members of the P_+, P_- subspaces as $v_+(\ell_+)$, $v_-(\ell_-)$, respectively, Eq. (26) then implies

$$\begin{aligned} -\Delta(\epsilon,\epsilon')v_\pm(\ell_\pm) &= -\Delta(\epsilon_\pm,0)v_\pm(\ell_\pm) \\ &= \ell_\pm v_\pm(\ell_\pm). \end{aligned} \tag{28}$$

Thus, it suffices to attain the eigensystems of the matrices $-\Delta(\epsilon_\pm,0)$. The characteristic polynomials of $-\Delta(\epsilon_\pm,0)$ are in fact doubly convex combinations in $\epsilon_\pm$ (see Appendix A for a derivation). The eigenvalues of $-\Delta(\epsilon_\pm,0)$ are respectively the roots of these two degree N polynomials:

$$\begin{aligned} \mathcal{P}_\pm &= (1-\epsilon_\pm)^2[(2\alpha_\pm - 2)\mathrm{U}_{N-1}(\alpha_\pm)] + \epsilon_\pm^2[\mathrm{U}_N(\alpha_\pm)] \\ &\quad + 2(1-\epsilon_\pm)\epsilon_\pm\big[\beta_\pm^{-1}\mathrm{T}_{2N+1}(\beta_\pm)\big], \end{aligned} \tag{29}$$

$$\text{for} \quad \alpha_\pm := 1 - \frac{\ell_\pm}{2}, \qquad \beta_\pm := \left(1 - \frac{\ell_\pm}{4}\right)^{1/2},$$

where T_k and U_k are the kth-order Chebyshev polynomials of the first and second kind [26–28] (the T_{2N+1} term is a polynomial in λ, even though the argument involves a square root, see Appendix A). The mth component of the (nonnormalized) eigenvector corresponding to eigenvalue $\ell_\pm$ can be expressed as

$$\begin{aligned} [v_\pm(\ell_\pm)]_m &= \epsilon_\pm[\mathrm{U}_{m-1}(\alpha_\pm)] \\ &\quad + (1-\epsilon_\pm)[\beta_\pm^{-1}\mathrm{T}_{2m-1}(\beta_\pm)], \end{aligned} \tag{30}$$

where $m = 1,\ldots,N$. Equations (29) and (30) give a complete description of eigenvalues/vectors of the inverse capacitance matrix [by making use of Eqs. (22) and (18)]. The reader may notice that the eigenvalues of the inverse capacitance matrix above do not depend on external flux: This dependence comes in when the eigenvalues are input into the Hamiltonian, which does depend on flux, to compute energies and wave functions of quantum states.

Before continuing, we address an important detail. Each of the polynomials $\mathcal{P}_+$ and $\mathcal{P}_-$ has N roots: Together, they have $2N$, which is double the number of eigenvalues. To obtain the N eigenvalues of $-\Delta(\epsilon,\epsilon')$, one computes all $2N$ roots, plugs them into the eigenvector formula in Eq. (30), and keeps only eigenvalues which produce eigenvectors with the correct symmetry. The N roots of $\mathcal{P}_+$ are to be plugged into the $v_+(\ell_+)$ formula, and only those eigenvalues which produce even vectors are kept. Similarly, the N roots of $\mathcal{P}_-$ are plugged into $v_-(\ell_-)$, and only those eigenvalues which produce odd vectors are kept. This procedure results in N eigenvalues/vectors, and these constitute the eigensystem of $-\Delta(\epsilon,\epsilon')$.

With the correct roots obtained, there is an alternative, simpler formula for the eigenvectors. Defining a vector-valued function $\tilde{v}(x)$ with components:

$$[\tilde{v}(x)]_m = \cos\left[(2m-1)\arcsin\sqrt{\frac{x}{4}}\right], \tag{31}$$

for $m = 1,\ldots,N$, then a nonnormalized eigenvector corresponding to even/odd eigenvalue $\ell_\pm$ is

$$P_\pm\tilde{v}(\ell_\pm). \tag{32}$$

The eigenvectors are thus seen to be even and odd superpositions of plane waves. With these expressions, one can show that, for even modes,

$$\mathcal{N}_\mu = \frac{8\sin\left(N\csc^{-1}\sqrt{\frac{4}{\ell_+}}\right)^2/\ell_+}{N + \csc\left(2\csc^{-1}\sqrt{\frac{4}{\ell_+}}\right)\sin\left(2N\csc^{-1}\sqrt{\frac{4}{\ell_+}}\right)}, \tag{33}$$

for the μth even eigenvalue ℓ_+ (including the zeroth eigenvalue), and $\mathcal{N}_\mu = 0$ for all odd modes. It is useful to expand $\mathcal{N}_\mu$ when ground capacitances are small. In this case, $\epsilon_+ \approx 0$, and the characteristic polynomial $\mathcal{P}_+ \approx (2\alpha_+ - 2)\mathrm{U}_{N-1}(\alpha_+)$. The roots of this polynomial are $0, 4\sin^2(\mu\pi/2N)$, for $\mu = 1,\ldots,N-1$, whose positions will be perturbed by ground capacitances to $0+\delta_0, 4\sin^2(\mu\pi/2N)+\delta_\mu$. One finds

$$\begin{aligned} \mathcal{N} &= N + \frac{\delta_0^2}{720}(-4N + 5N^3 - N^5) + O(\delta_0^3), \\ \mathcal{N}_\mu &= \delta_\mu^2\frac{N}{32}\csc\left(\frac{\mu\pi}{2N}\right)^4\sec\left(\frac{\mu\pi}{2N}\right)^2 + O(\delta_\mu^3), \end{aligned} \tag{34}$$

for even modes, while for odd modes, $\mathcal{N}_\mu$ always vanishes.

We now provide a numerical demonstration of our formulas in Fig. 2. Motivated by an experiment reaching

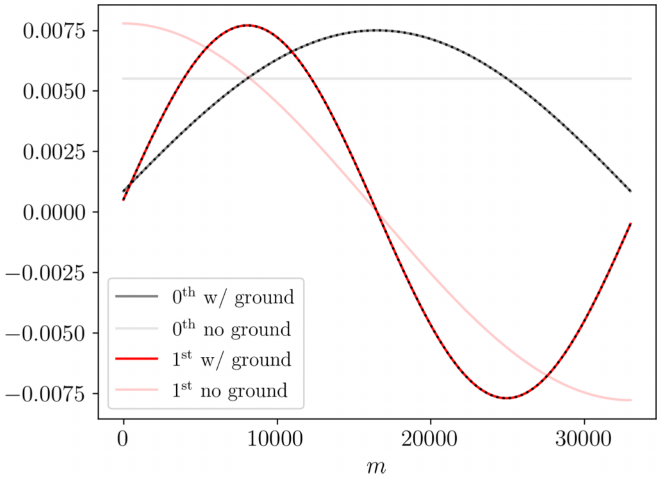

FIG. 2. Two lowest array mode eigenvectors of an $N = 33\,000$ array with capacitances of Eq. (35). The vertical axis is dimensionless and is proportional to the voltage profile across the array. Opaque/transparent curves include/neglect ground capacitance respectively. Dotted black lines result from numerically diagonalizing the inverse capacitance matrix.

$N = 33\,000$ [29], we consider a very long $N = 33\,000$ array, where ground effects are large, with capacitances:

$$\left(C^a, C^b, C_g^a, C_g^b\right) = (19.37, 5.23, 0.01, 3.87)\ [\text{fF}], \tag{35}$$

taken from Appendix F of Ref. [16] (we convert the reported charging energies to capacitances via $E_C = e^2/2C$). We solve for the lowest two modes of $\mathbb{C}^{-1}$ using our exact result and compare against exact diagonalization. The dotted black lines in the figure are obtained by numerically diagonalizing the inverse capacitance matrix, and their agreement with the red and gray curves, obtained from Eq. (30), demonstrates our formulas are correct. The transparent curves are the approximate eigenvectors of Ref. [16], obtained by dropping ground capacitances (i.e., setting $C_3 = C_4 = 0$). The difference between transparent and opaque curves indicates that ground capacitances substantially modify mode profiles in long arrays.

We conclude this section by showing how the preceding results apply to grounded (rather than differential) fluxonium devices. Consider a grounded fluxonium device with N array junctions, Lagrangain given by Eqs. (2)–(4), and capacitances C^a, C^b, C_g^a, C_g^b. Then all that changes in the derivation of the quantum Hamiltonian of this circuit is that $\dot{\tau} = 0$ from the outset. The effect of this change is to eliminate C_4 from the capacitance matrix, so that $\mathbb{C} = C_1 + C_2 + C_3$. The eigensystem of this new capacitance matrix can be solved with similar methods to the differential case. One finds that

$$\frac{1}{C_2 + C_3} = \frac{1}{C_g^a}\begin{bmatrix} 1 & -1 & & & \\ -1 & 2 & -1 & & \\ & \ddots & \ddots & \ddots & \\ & & -1 & 2 & -1 \\ & & & -1 & 1+\delta \end{bmatrix}$$
$$:= \frac{-\Delta(\delta)}{C_g^a}, \tag{36}$$

where $\delta = C_g^a/(C^b + C_g^b)$ and where we have defined a new $N \times N$ matrix $-\Delta(\delta)$.

The eigensystem of Eq. (36) can be obtained by noticing that it is embedded in that of a differential device with $2N$ array junctions and small junction capacitance $C^b/2$. In this case,

$$-\Delta(\epsilon_+, 0)P_+ = \frac{1}{2}\begin{bmatrix} -\mathbb{F}\Delta(\delta)\mathbb{F} & -\mathbb{F}\Delta(\delta) \\ -\Delta(\delta)\mathbb{F} & -\Delta(\delta) \end{bmatrix}, \tag{37}$$

where it is understood that the matrix on the left-hand side is $2N \times 2N$ and the blocks on the left are $N \times N$. The even eigenvectors of the $2N$-sized system can be written as $v_{2N} = [\mathbb{F}v_N \quad v_N]$, and one can show that $-\Delta(\epsilon_+, 0)P_+ v_{2N} = \lambda v_{2N}$ implies $-\Delta(\delta)v_N = \lambda v_N$. Thus, the eigenvectors of the grounded system with N array junctions and small junction capacitance C^b are the first half of the eigenvectors of the differential system with $2N$ array junctions and small junction capacitance $C^b/2$, and the eigenvalues between the two cases are the same.

This same conclusion can be reached from symmetry arguments [14,20]. The even modes of a differential device with $2N$ array junctions have zero voltage at the midpoint of the circuit. Rewriting the small junction capacitor as two equal capacitors in series and noting the reflection symmetry about the midpoint shows that, from the point of view of the even modes, the first N junctions of the circuit is indistinguishable from a grounded device.

IV. APPROXIMATION SCHEME

The formulas of Eqs. (29) and (30) for the eigensystem of $\mathbb{C}^{-1}$ are exact. However, it may be useful to work with approximate eigensystems with simple expressions requiring no root finding for speed and intuition. We presently provide such a scheme.

The approximate eigenvalues of $\mathbb{C}^{-1}$ are

$$\lambda_0 = \left[C^a + \frac{C_g^a}{\ell_0}\right]^{-1}$$
$$\lambda_\mu^{\text{even}} = \left[C^a + \frac{C_g^a}{\ell_\mu^{\text{even}}}\right]^{-1}$$
$$\lambda_\mu^{\text{odd}} = \left[C^a + \frac{C_g^a}{\ell_\mu^{\text{odd}}}\right]^{-1}, \tag{38}$$

where

$$\ell_0 = \left[\left(\frac{N^2}{12} - \frac{N}{4} + \frac{1}{6}\right) + \frac{NC^b}{C_g^a} + \frac{N}{2}\frac{C_g^b}{C_g^a}\right]^{-1}$$
$$\ell_\mu^{\text{even}} = 4\sin^2\left(\frac{\mu\pi}{2N}\right) + \frac{4}{N}\cos^2\left(\frac{\mu\pi}{2N}\right)\frac{C_g^a}{2C^b + C_g^b}$$
$$\ell_\mu^{\text{odd}} = 4\sin^2\left(\frac{\mu\pi}{2N}\right) + \frac{4}{N}\cos^2\left(\frac{\mu\pi}{2N}\right)\frac{C_g^a}{C_g^b}, \tag{39}$$

and the approximate eigenvectors of $\mathbb{C}^{-1}$ are

$$\begin{aligned} v_0 &= P_+\tilde{v}(\ell_0) \\ v_\mu^{\text{even}} &= P_+\tilde{v}\left(\ell_\mu^{\text{even}}\right) \\ v_\mu^{\text{odd}} &= P_-\tilde{v}\left(\ell_\mu^{\text{even}}\right), \end{aligned} \tag{40}$$

where $\mu = 1, \dots, N-1$. The $\mathcal{N}, \mathcal{N}_\mu$ corresponding to these approximate eigenvectors can be obtained by substituting $\ell_0, \ell_\mu^{\text{even}}$ into Eq. (33) or approximated by Eq. (34). For the odd modes, $\mathcal{N}_\mu = 0$.

We arrive at this approximation scheme in the following way. First, the approximate eigenvectors are simply the exact eigenvectors of $-\Delta(\epsilon, \epsilon')$ (and therefore $\mathbb{C}^{-1}$) evaluated at approximate eigenvalues. This choice retains the correct symmetry and wavelike profile of the exact solution but uses an approximate wave number. To estimate the eigenvalues of $\mathbb{C}^{-1}$, we leverage the eigenvectors of Ref. [16], namely:

$$\begin{aligned} (\mathbf{v}_0)_m &= N^{-1/2} \\ (\mathbf{v}_\mu)_m &= \sqrt{\frac{2}{N}}\cos\left[\frac{\pi\mu}{N}\left(m-\frac{1}{2}\right)\right], \end{aligned} \tag{41}$$

which can be shown to be the limit of the exact eigenvectors as ground capacitances go to zero. We then separate two cases: the lowest eigenvalue and the rest of them. For the latter, we compute

$$\mathbf{v}_\mu^\dagger\left[\frac{-\Delta(\epsilon, \epsilon, \epsilon', N)}{C_g^a}\right]\mathbf{v}_\mu, \tag{42}$$

which is an estimate of the μth eigenvalue of $(C_2 + C_3 + C_4)^{-1}$. We then use Eq. (22) to relate this eigenvalue estimate to one for the full $\mathbb{C}^{-1}$. Depending whether $\mathbf{v}_\mu$ is an even or odd mode, either $\epsilon_+ = C_g^a/(2C^b + C_g^b)$ or $\epsilon_- = C_g^a/C_g^b$ appears in the calculation, and this produces the different dependencies in Eq. (39). The dependence/independence of even/odd vectors on C^b is expected from symmetry, and it is a strength of our scheme this feature is captured. Furthermore, since ground capacitances are typically much smaller than junction capacitances, $\epsilon_+ << \epsilon_-$, and one therefore expects better estimates for the even modes than the odd.

Repeating the above procedure with $\mathbf{v}_0$, one obtains $(C^a + NC^b + C_g^b N/2)^{-1}$ as an estimate of the lowest eigenvalue of $\mathbb{C}^{-1}$. A tighter bound can be obtained, however, by observing that the lowest eigenvalue of $\mathbb{C}^{-1}$ is equal to the inverse of the highest eigenvalue of $\mathbb{C}$. Thus, the lowest eigenvalue of $\mathbb{C}^{-1}$ is bounded from above by $\lambda_0 := (v_0^\dagger \mathbb{C} v_0)^{-1}$, which is equal to the expression in Eq. (38). Since $\lambda_0 < (C^a + NC^b + C_g^b N/2)^{-1}$, it is a tighter bound, and we use it. Previous work arrived at this same estimate [16]. Finally, we have shown that solving for the roots of the exact solution Eq. (29) to first order in $\epsilon_\pm$ yields the same approximate eigenvalues as the present method.

We now give an example to illustrate the utility of the approximation scheme. For the rest of this section, we consider systems with variable N but with capacitances fixed to those listed in Eq. (35), which we reproduce here:

$$\left(C^a, C^b, C_g^a, C_g^b\right) = (19.37, 5.23, 0.01, 3.87)\ [\text{fF}]. \tag{43}$$

In Fig. 3(a), we plot the fractional error of the first even parity array mode λ_2 for $N \leqslant 400$, where fractional error is defined as $100 \times |(\lambda_{\text{exact}} - \lambda_{\text{approx}})/\lambda_{\text{exact}}|$. The estimate is quite good, with $<1\%$ error by $N = 400$. In the figure, we also compare with perturbation theory, which approximates the full inverse capacitance matrix by the first few terms in the geometric series:

$$\frac{1}{C_1 + C_2 + C_g} = \sum_{k=0}^{\infty}(-1)^k \frac{1}{C_1 + C_2}\left[C_g \frac{1}{C_1 + C2}\right]^k,$$

where $C_g = C_3 + C_4$ [16,17]. In the figure LO and N2LO mean to cut off the infinite sum at $k = 0, 2$, respectively. At leading order, the superinductance mode eigenvalue equals $1/(C^a + NC^b)$, while the array mode eigenvalues are degenerate with eigenvalue $1/C^a$. We skip NLO ($k = 1$) because the series exhibits an alternating behavior which renders the NLO estimate quite poor. Figure 3(a) shows our approximation scheme is more accurate than perturbation theory. Since our approximation scheme requires only a function call rather than matrix multiplications, it is also cheaper.

In Fig. 3(b), we compare $\lambda_0, \lambda_1, \lambda_2, \lambda_3$ to the exact result for $N \leqslant 1,000$. The estimates are seen to have at worst a $\sim$14% error; this occurs for the first odd parity mode which has an anomalously large error. All other modes are extremely well estimated, with $<2\%$ error by $N = 1000$. On average, the error of the odd modes is larger than the error for the even modes. This can be traced back to the fact that the correction to the free Laplacian eigenvalue for odd modes is proportional to C_g^a/C_g^b, while the correction for even modes is proportional to $C_g^a/(2C^b + C_g^b)$, which is much smaller. Figure 3(c) compares first four exact and approximate eigenvectors at $N = 1000$. The parity and wavelike nature of eigenvectors are baked into the approximation scheme, with only the estimated wave number slightly incorrect. In Fig. 3(d), we fix $N = 1000$ and plot the spectrum of $\mathbb{C}^{-1}$. The low modes have the highest error; however, as indicated by the inset, the entire spectrum is well approximated.

We conclude this section by noting that, while this approximation scheme is quite accurate, it does not capture the correct asymptotic behavior of eigenvalues at large N and will become inaccurate at large enough arrays. Computing eigenvalues for array lengths up to $N = 250\,000$, we find strong evidence that the asymptotic scaling of eigenvalues is N^{-2}, a feature noted previously [30]. While our superinductance mode estimate scales as N^{-2}, the array mode estimates scale as N^{-1}. On very large arrays, we suggest the following alternative estimate, which has the correct asymptotic scaling:

$$\begin{aligned} \left(\mathbf{v}_\mu^\dagger \mathbb{C} \mathbf{v}_\mu\right)^{-1} = \Bigg\{ & C^a + \frac{C_g^a}{4}\sin^{-2}\left(\frac{\pi\mu}{2N}\right) \\ & - \frac{[1-(-1)^\mu]^2 {C_g^a}^2}{2C_g^b + (N-1)C_g^a}\frac{\cot^2\left(\frac{\pi\mu}{2N}\right)\csc^2\left(\frac{\pi\mu}{2N}\right)}{8N}\Bigg\}^{-1}. \end{aligned} \tag{44}$$

V. CONCLUSIONS

In this paper, we presented an exact solution for the array modes of fluxonium in the absence of array disorder.

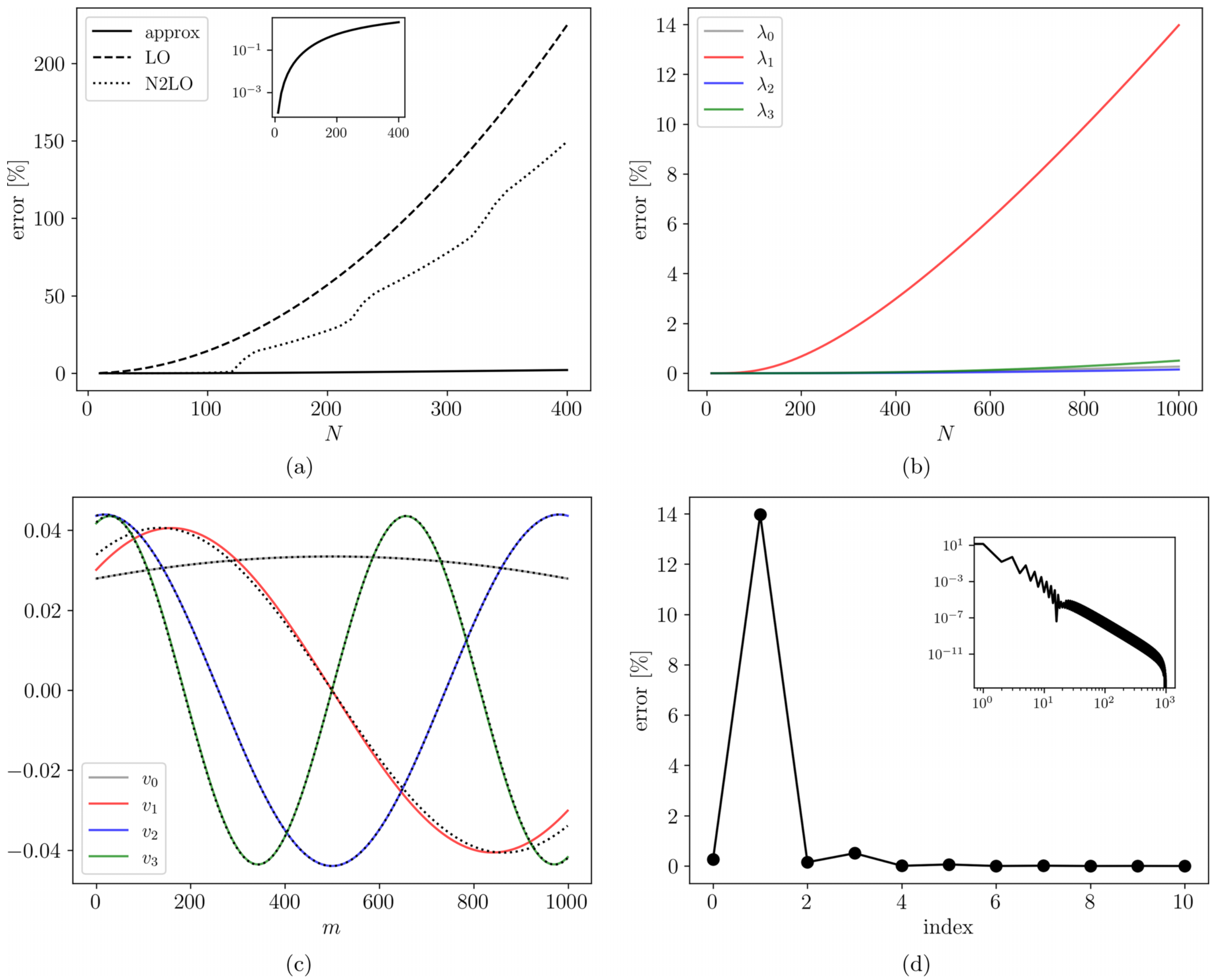

FIG. 3. Approximation scheme performance. (a) Fractional error of λ_2 in different approximation schemes. Our scheme is labeled "approx," while LO and N2LO indicate leading- and next-to-next-to-leading-order perturbation theory. The inset shows the logarithm of the fractional error of the approximation scheme. (b) Fractional error of our approximation scheme for the lowest four eigenvalues of $\mathbb{C}^{-1}$ as a function of the number of array junctions N. (c) Exact and approximate eigenvectors of four lowest modes at $N = 1000$. The vertical axis is dimensionless. Colored lines are the approximate eigenvectors, while the dotted black lines are the exact eigenvectors. (d) Fractional error of eigenvalues at $N = 1000$ in our approximation scheme. The horizontal axis indexes eigenvalues. Points show the lowest eigenvalues, while the inset shows the whole spectrum.

Array mode energies and spatial profiles are determined by the eigenvalues and eigenvectors of the inverse capacitance matrix, which we have explicitly solved for. The eigenvalues are the roots of a doubly convex combination of Chebyshev polynomials, while the eigenvectors are plane waves. These results extend known formulas for the array mode spectrum in the absence of ground capacitances [16].

In the course of developing this solution, it was shown that the inverse capacitance matrix is related to a discrete Laplace operator with Robin-Robin boundary conditions. This intermediate result has practical utility because it shows that, while the capacitance matrix itself is dense, its spectrum can be computed from a sparse matrix.

Reflection symmetry of the circuit about its midpoint is essential in our analysis: It organizes array modes into even and odd parity subspaces and simplifies the mathematical steps required to find the eigensystem. The even array modes were seen to couple to the superinductance mode through the small junction with a magnitude controlled by the array mode normalizations $\mathcal{N}_\mu$. These couplings produce corrections to the circuit Hamiltonian which vary exponentially with the mode impedances [12], and to assist in their quantification, we have provided both exact and approximate expressions for the normalizations. We then related our results for a differential device to a grounded one, showing that the array modes of a grounded device of length N with small junction capacitance C^b are equal to the first half of the even modes of a length $2N$ floating fluxonium with small junction capacitance $C^b/2$.

We provided a simple approximation scheme for the eigensystem of the inverse capacitance matrix requiring no Chebyshev polynomials. Eigenvalues are approximated by simple analytic expressions, while eigenvectors are plane waves. For arrays <1000 junctions long, all eigenvalues except the first odd array mode are estimated to better than 2%. The eigenvector approximation scheme involves substituting into the exact formula an approximate wave number, which approximate eigenvectors well. Our scheme outperforms perturbation theory in both speed and accuracy.

Here, we focus on only a small aspect of the physics of fluxonium. It will be interesting to explore the consequences of our formulas on large arrays. It will also be interesting to explore applications of our method to other qubits containing superinductances such as $0-\pi$. The challenge in this case would be the presence of a second superinductor and couplings between their respective array modes.

ACKNOWLEDGMENTS

S.S. is supported by the NIST/NRC Postdoctoral Associateship Program. N.C.W. is supported by the U.S. Department of Energy, Office of Science under Grant Contracts No. DE-SC0011090 and No. DE-SC0021006, the Simons Foundation Grant No. 994314 (Simons Collaboration on Confinement and QCD Strings), and the U.S. Department of Energy, Office of Science, National Quantum Information Science Research Centers, Co-Design Center for Quantum Advantage under Contract No. DE-SC0012704. M.H. was supported by an appointment to the Intelligence Community Postdoctoral Research Fellowship Program at the Massachusetts Institute of Technology administered by Oak Ridge Institute for Science and Education (ORISE) through an interagency agreement between the U.S. Department of Energy and the Office of the Director of National Intelligence (ODNI). This research was funded in part by the U.S. Army Research Office under Award No. W911NF-23-1-0045.

APPENDIX A: CHARACTERISTIC POLYNOMIAL DERIVATION

In this Appendix, we derive the characteristic polynomial of the $N \times N$ matrix:

$$-\Delta(\epsilon,0)=\begin{bmatrix}1+\epsilon & -1 & & & \\ -1 & 2 & -1 & & \\ & \ddots & \ddots & \ddots & \\ & & -1 & 2 & -1 \\ & & & -1 & 1+\epsilon\end{bmatrix}, \quad \text{(A1)}$$

for general ϵ, N. We do this by considering an auxiliary matrix:

$$-\Delta(\epsilon):=\begin{bmatrix}1 & -1 & & & \\ -1 & 2 & -1 & & \\ & \ddots & \ddots & \ddots & \\ & & -1 & 2 & -1 \\ & & & -1 & 1+\epsilon\end{bmatrix}, \quad \text{(A2)}$$

explaining at the end how to extend the result to Eq. (A1). Denote this characteristic polynomial by

$$P(\lambda,\epsilon):=\det[-\Delta(\epsilon)-\lambda\mathbb{1}]. \quad \text{(A3)}$$

The recurrence relation for the determinant of a tridiagonal matrix [31,32] gives

$$P(\lambda,\epsilon)=(1+\epsilon-\lambda)p_{N-1}-p_{N-2}, \quad \text{(A4)}$$

where p_i is the determinant of an $i \times i$ matrix:

$$p_i=\det\begin{bmatrix}1-\lambda & -1 & & & \\ -1 & 2-\lambda & -1 & & \\ & \ddots & \ddots & \ddots & \\ & & -1 & 2-\lambda & -1 \\ & & & -1 & 2-\lambda\end{bmatrix}. \quad \text{(A5)}$$

Each p_i is a difference of Chebyshev polynomials of the second kind [27]:

$$p_i=\mathrm{U}_{i-1}(\alpha)-\mathrm{U}_{i-2}(\alpha), \quad \text{for} \quad \alpha=1-\frac{\lambda}{2}. \quad \text{(A6)}$$

The characteristic polynomial thus reads

$$P(\lambda,\epsilon)=(1+\epsilon-\lambda)[\mathrm{U}_{N-1}(\alpha)-\mathrm{U}_{N-2}(\alpha)] \\ -[\mathrm{U}_{N-2}(\alpha)-\mathrm{U}_{N-3}(\alpha)]. \quad \text{(A7)}$$

The next steps are as follows: Rearrange the terms of Eq. (A7) to extract a term proportional to $(1-\epsilon)$ and a second term proportional to ϵ. Both of these terms will contain sums of $\mathrm{U}_i(\alpha)-\mathrm{U}_{i-1}(\alpha)$, where $i=N-1, N-2$. We proceed to eliminate all instances of $\mathrm{U}_{N-3}(\alpha)$ via the recurrence relation (DLMF, sec. 18.9 [26]):

$$\mathrm{U}_{N-3}(\alpha)=2\alpha\,\mathrm{U}_{N-2}(\alpha)-\mathrm{U}_{N-1}(\alpha). \quad \text{(A8)}$$

The Chebyshev polynomial of the first kind T_k is then introduced using a combination of the two formulas (eq. 3 of sec. 10.11, p. 184 [33], DLMF, sec. 3.11.7 [26], and Refs. [27,28]):

$$\mathrm{T}_n(x)=\mathrm{U}_n(x)-x\,\mathrm{U}_{n-1}(x), \\ \mathrm{T}_{n+1}(x)=2x\,\mathrm{T}_n(x)-T_{n-1}(x). \quad \text{(A9)}$$

In the previous expression for $P(\lambda,\epsilon)$, the following substitution is made:

$$(2\alpha-2)\mathrm{U}_{N-1}(\alpha)+\{\mathrm{U}_{N-1}(\alpha)-\mathrm{U}_{N-2}(\alpha)\}=\frac{1}{\beta}\mathrm{T}_{2N+1}(\beta), \quad \text{(A10)}$$

where $\beta=\sqrt{1-\lambda/4}$. This yields the characteristic polynomial in Eq. (29), which in the current special case reads

$$P=[(2\alpha-2)\mathrm{U}_{N-1}(\alpha)](1-\epsilon)+[\beta^{-1}\mathrm{T}_{2N+1}(\beta)]\epsilon. \quad \text{(A11)}$$

The same steps can be followed for the characteristic polynomial of $-\Delta(\epsilon,0)$, which yields

$$P=(1-\epsilon)^2[(2\alpha-2)\mathrm{U}_{N-1}(\alpha)]+\epsilon^2[\mathrm{U}_N(\alpha)] \\ +2(1-\epsilon)\epsilon[\beta^{-1}\mathrm{T}_{2N+1}(\beta)]. \quad \text{(A12)}$$

APPENDIX B: EIGENVECTOR DERIVATION

In this Appendix, we derive the eigenvectors of $-\Delta(\epsilon,0)$, i.e., Eq. (30), reproduced here:

$$[v(\lambda)]_m=\epsilon[\mathrm{U}_{m-1}(\alpha)]+(1-\epsilon)[\beta^{-1}\mathrm{T}_{2m-1}(\beta)]. \quad \text{(B1)}$$

In this expression, λ is a fixed eigenvalue determined as a root of the characteristic polynomial in Eq. (29), and $\alpha = 1 - \lambda/2$, $\beta = \sqrt{1 - \lambda/4}$, as before. The derivation relies on the fact that the components $[v(\lambda)]_m$ satisfy the same iteration scheme as subdeterminants of $-\Delta(\epsilon, 0)$.

More precisely, the recurrence relation for $[v(\lambda)]_m$ is found by unpacking the matrix eigenvalue problem and is particularly simple since $-\Delta(\epsilon, 0)$ is tridiagonal:

$$\begin{aligned} [v(\lambda)]_2 &= (1 + \epsilon - \lambda)[v(\lambda)]_1 \\ [v(\lambda)]_k &= (2 - \lambda)[v(\lambda)]_{k-1} - [v(\lambda)]_{k-2}, \\ &\quad 2 < k < N \\ (1 + \epsilon - \lambda)[v(\lambda)]_N &= [v(\lambda)]_{N-1}. \end{aligned} \tag{B2}$$

We may assume, without loss of generality, that $v_1 = 1$ since the state can be normalized arbitrarily without changing the eigenvalue equation. In addition to this, we may define

$$[v(\lambda)]_{N+1} \equiv 0. \tag{B3}$$

The scheme in Eqs. (B2) and (B3) is in fact identical to the recurrence relation for subdeterminants of $[-\Delta(\epsilon) - \lambda]$. That is, the values:

$$\det{}_k[-\Delta(\epsilon) - \lambda], \qquad k = 0, 1, \ldots, N, \tag{B4}$$

corresponding to the determinant of the $k \times k$ matrix formed from the first k rows/columns of $[-\Delta(\epsilon) - \lambda]$. For any matrix M, we define $\det_0[M] = 0$, and since λ is an eigenvalue, it follows that

$$\det{}_N[-\Delta(\epsilon, 0) - \lambda] = 0.$$

The recurrence relation for determinants of tridiagonal matrices [34] can then be used to show that the scheme Eq. (B2) also holds for $\det_k[-\Delta(\epsilon) - \lambda]$; in fact,

$$[v(\lambda)]_k = \det{}_{k-1}[-\Delta(\epsilon) - \lambda], \qquad k = 2, \ldots, N.$$

It can be shown that these subdeterminants in Eq. (B4) have already been derived in Eq. (A11), so we have derived the formula for the eigenvectors.

We include in the Supplemental Material a Mathematica notebook [35]. This notebook implements the exact solution, checks many of the detailed intermediate steps of the proof, and provides simple implementations of the approximate solutions. This code is not optimized in any way: our desire is simply to provide a starting point for anyone who wishes to use these results.

[1] P. Krantz, M. Kjaergaard, F. Yan, T. P. Orlando, S. Gustavsson, and W. D. Oliver, A quantum engineer's guide to superconducting qubits, Appl. Phys. Rev. **6**, 021318 (2019).

[2] N. Crescini, S. Cailleaux, W. Guichard, C. Naud, O. Buisson, K. W. Murch, and N. Roch, Evidence of dual Shapiro steps in a Josephson junction array, Nat. Phys. **19**, 851 (2023).

[3] A. Roy and M. Devoret, Introduction to parametric amplification of quantum signals with Josephson circuits, C. R. Phys. **17**, 740 (2016).

[4] N. Mehta, R. Kuzmin, C. Ciuti, and V. E. Manucharyan, Down-conversion of a single photon as a probe of many-body localization, Nature (London) **613**, 650 (2023).

[5] V. Manucharyan, Superinductance, Ph.D. thesis, Yale University, 2012.

[6] N. A. Masluk, I. M. Pop, A. Kamal, Z. K. Minev, and M. H. Devoret, Microwave characterization of Josephson junction arrays: Implementing a low loss superinductance, Phys. Rev. Lett. **109**, 137002 (2012).

[7] V. E. Manucharyan, J. Koch, L. I. Glazman, and M. H. Devoret, Fluxonium: Single cooper-pair circuit free of charge offsets, Science **326**, 113 (2009).

[8] W. Smith, A. Kou, X. Xiao, U. Vool, and M. Devoret, Superconducting circuit protected by two-Cooper-pair tunneling, npj Quantum Inf. **6**, 8 (2020).

[9] A. Gyenis, P. S. Mundada, A. Di Paolo, T. M. Hazard, X. You, D. I. Schuster, J. Koch, A. Blais, and A. A. Houck, Experimental realization of a protected superconducting circuit derived from the 0–π qubit, PRX Quantum **2**, 010339 (2021).

[10] V. E. Manucharyan, N. A. Masluk, A. Kamal, J. Koch, L. I. Glazman, and M. H. Devoret, Evidence for coherent quantum phase slips across a Josephson junction array, Phys. Rev. B **85**, 024521 (2012).

[11] A. Mizel and Y. Yanay, Right-sizing fluxonium against charge noise, Phys. Rev. B **102**, 014512 (2020).

[12] A. Di Paolo, T. E. Baker, A. Foley, D. Sénéchal, and A. Blais, Efficient modeling of superconducting quantum circuits with tensor networks, npj Quantum Inf. **7**, 11 (2021).

[13] M. T. Randeria, T. M. Hazard, A. Di Paolo, K. Azar, M. Hays, L. Ding, J. An, M. Gingras, B. M. Niedzielski, H. Stickler, , Dephasing in fluxonium qubits from coherent quantum phase slips, arXiv:2404.02989.

[14] L. B. Nguyen, Y.-H. Lin, A. Somoroff, R. Mencia, N. Grabon, and V. E. Manucharyan, High-coherence fluxonium qubit, Phys. Rev. X **9**, 041041 (2019).

[15] H. Zhang, S. Chakram, T. Roy, N. Earnest, Y. Lu, Z. Huang, D. K. Weiss, J. Koch, and D. I. Schuster, Universal fast-flux control of a coherent, low-frequency qubit, Phys. Rev. X **11**, 011010 (2021).

[16] D. G. Ferguson, A. A. Houck, and J. Koch, Symmetries and collective excitations in large superconducting circuits, Phys. Rev. X **3**, 011003 (2013).

[17] G. Viola and G. Catelani, Collective modes in the fluxonium qubit, Phys. Rev. B **92**, 224511 (2015).

[18] T. M. Hazard, A. Gyenis, A. Di Paolo, A. T. Asfaw, S. A. Lyon, A. Blais, and A. A. Houck, Nanowire superinductance fluxonium qubit, Phys. Rev. Lett. **122**, 010504 (2019).

[19] N. E. Frattini, U. Vool, S. Shankar, A. Narla, K. M. Sliwa, and M. H. Devoret, 3-wave mixing josephson dipole element, Appl. Phys. Lett. **110**, 222603 (2017).

[20] L. Ding, M. Hays, Y. Sung, B. Kannan, J. An, A. Di Paolo, A. H. Karamlou, T. M. Hazard, K. Azar, D. K. Kim, High-fidelity, frequency-flexible two-qubit fluxonium gates with a transmon coupler, Phys. Rev. X **13**, 031035 (2023).

[21] F. Yan, S. Gustavsson, A. Kamal, J. Birenbaum, A. P. Sears, D. Hover, T. J. Gudmundsen, D. Rosenberg, G. Samach, S. Weber, The flux qubit revisited to enhance coherence and reproducibility, Nat. Commun. **7**, 12964 (2016).
[22] M. H. Devoret, Quantum fluctuations in electrical circuits, in *Quantum Fluctuations*, edited by E. G. S. Reynaud and J. Zinn-Justin (Elsevier, Amsterdam, 1997), pp. 351–386.
[23] A. Caldeira and A. Leggett, Quantum tunnelling in a dissipative system, Ann. Phys. **149**, 374 (1983).
[24] G. Burkard, R. H. Koch, and D. P. DiVincenzo, Multilevel quantum description of decoherence in superconducting qubits, Phys. Rev. B **69**, 064503 (2004).
[25] Here and throughout, we drop unimportant constant terms.
[26] DLMF, NIST Digital Library of Mathematical Functions, https://dlmf.nist.gov/, Release 1.1.12 of 2023-12-15, F. W. J. Olver, A. B. Olde Daalhuis, D. W. Lozier, B. I. Schneider, R. F. Boisvert, C. W. Clark, B. R. Miller, B. V. Saunders, H. S. Cohl, and M. A. McClain, eds.
[27] E. W. Weisstein, Chebyshev polynomial of the second kind. From MathWorld—A Wolfram Web Resource.
[28] E. W. Weisstein, Chebyshev polynomial of the first kind. From MathWorld—A Wolfram Web Resource.
[29] R. Kuzmin, R. Mencia, N. Grabon, N. Mehta, Y.-H. Lin, and V. E. Manucharyan, Quantum electrodynamics of a superconductor-insulator phase transition, Nat. Phys. **15**, 930 (2019).
[30] G. Rastelli, I. M. Pop, and F. W. J. Hekking, Quantum phase slips in Josephson junction rings, Phys. Rev. B **87**, 174513 (2013).
[31] M. E. El-Mikkawy, On the inverse of a general tridiagonal matrix, Appl. Math. Comput. **150**, 669 (2004).
[32] R. A. Horn and C. R. Johnson, *Matrix Analysis* (Cambridge University Press, Cambridge, 1985).
[33] H. Bateman, *Higher Transcendental Functions* (McGraw-Hill Book Company, New York, 1953), Vol. I–III.
[34] K. B. Petersen and M. S. Pedersen, The matrix cookbook (2012), version 20121115, https://www2.imm.dtu.dk/pubdb/edoc/imm3274.pdf.
[35] See Supplemental Material at http://link.aps.org/supplemental/10.1103/PhysRevB.110.125404 for a Mathematica notebook.